RSC Advances

This is an *Accepted Manuscript*, which has been through the Royal Society of Chemistry peer review process and has been accepted for publication.

Accepted Manuscripts are published online shortly after acceptance, before technical editing, formatting and proof reading. Using this free service, authors can make their results available to the community, in citable form, before we publish the edited article. This *Accepted Manuscript* will be replaced by the edited, formatted and paginated article as soon as this is available.

You can find more information about *Accepted Manuscripts* in the Information for Authors.

Please note that technical editing may introduce minor changes to the text and/or graphics, which may alter content. The journal's standard Terms & Conditions and the Ethical guidelines still apply. In no event shall the Royal Society of Chemistry be held responsible for any errors or omissions in this *Accepted Manuscript* or any consequences arising from the use of any information it contains.

ROYAL SOCIETY OF CHEMISTRY

www.rsc.org/advances

Table of Contents

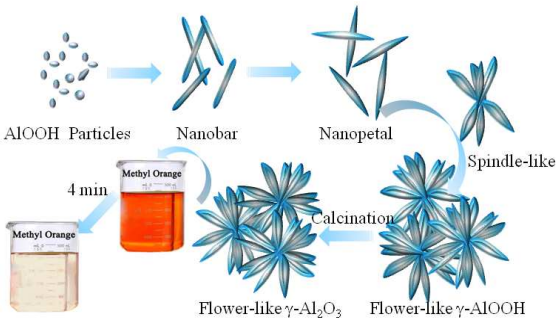

Highlights: Facile fabrication of novel flower-like γ-Al_2O_3 with enhanced adsorption performance involving with contaminants

RSC Advances Accepted Manuscript

Journal Name

RSCPublishing

ARTICLE

Self-Assembly of Flower-like γ-AlOOH and γ-Al_2O_3 with Hierarchical Nanoarchitectures and Enhanced Adsorption Performance towards Methyl Orange

Cite this: DOI: 10.1039/x0xx00000x

Received 00th January 2012,
Accepted 00th January 2012

DOI: 10.1039/x0xx00000x

www.rsc.org/

Jinchun Xiao[a,b], Honghai Ji[b], Zhiqi Shen[b], Weiya Yang[b], Changyou Guo[b], Shaojun Wang[b], Xiwen Zhang[b], Rong Fu[a,b] and Fengxiang Ling[b*]

Abstract: A novel flower-like γ-AlOOH and γ-Al_2O_3 with hierarchical Nanoarchitectures were successfully synthesized via the assembly of P123 and aluminium chloride with the urea being used as precipitating agent under hydrothermal conditions. The influence in morphology control were studied by altering the amount of P123 (V_{p123}) and molar ratio of $CO(NH_2)_2/Al^{3+}$ (R_{UAl}), implying that the increasing R_{UAl} could lead to the crystal growth in the form of nanofilms or nanostrips and the addition of P123 could have the morphology-alteration impact to 3D hierarchical architectures, and the possible formation mechanism were carefully studied. Further adsorption investigation indicates that the flower-like γ-Al_2O_3 exhibit an enhanced adsorption performance towards Methyl orange as a result of the unique hierarchical structure, and the addition of P123 also has an drastic effect on the surface acidity of the as-prepared flower-like γ-Al_2O_3.

Introduction

In the last decades, metal oxides with hierarchical structures have drawn more attention for their nanometre-sized building blocks and overall micrometre-sized structure with the increasing of varied applications ranging from adsorption, catalysis, energy conversion and storage to drug delivery, nanotechnology and biotechnology[1-4]. Alumina and aluminium oxide hydroxides nanomaterials with heterogeneous hierarchical nanostructures have been investigated extensively for scientific and industrial applications[5-13] due to their novel properties and promising applications. Especially, γ-AlOOH and γ-Al_2O_3 are used widely as catalysts, catalyst supports, adsorbents, ceramics, abrasives and filters[14-16].

Up to now, various hierarchical structured Boehmite and γ-Al_2O_3, such as nanotubes[17], nanofibers[18], nanorods[19], nanowire[20], nanoplatelets and nanowires[21], nanostructured microspheres[22], hollow microspheres[23-25] have been successfully achieved by various methods. Zhang et al.[26] have synthesized a flower-like three-dimensional (3D) nanoarchitectures by using anhydrate $AlCl_3$, during the synthetic process the ethanol-water solution were selected to slow down the strong hydrolyzation of the anhydrate $AlCl_3$.

However, not only the novel properties and hierarchical structures have been paid attention to but also the environmental problems involving water treatment. Despite the above-mentioned successful demonstrations, it is still a challenge to obtain γ-AlOOH or γ-Al_2O_3 with unique morphology and enhanced physicochemical properties, which would possess unique properties in the applications of water contamination treatment. Herein, A novel flower-like γ-AlOOH and γ-Al_2O_3 3D nanoarchitectures were successfully synthesized by hydrothermal method, and the effect on the morphology of the molar ratio of $CO(NH_2)_2/Al^{3+}$ (R_{UAl}) and the amount of Poly (ethylene glycol)-block-poly (propylene-glycol)-block-poly (ethylene glycol) (P123) were also carefully studied. On the basis of the control experiments and time-dependent experiments, we proposed a possible formation mechanism of the novel flower-like nanoarchitectures. Moreover, the as-prepared γ-Al_2O_3 was found to have an enhanced adsorption performance toward Methyl orange with a rapid adsorption rate, indicating their promising applications in water contamination treatment.

Experiment section

Synthesis of flower-like 3D hierarchical nanoarchitectures

All chemicals were of analytical grade reagents and used as received without further purification. In a typical synthesis

RSC Advances Accepted Manuscript

experiment, all experiments were performed under air atmosphere, 0.05 M aluminium chloride ($AlCl_3 \cdot 6H_2O$) and 0.075 M urea ($CO(NH_2)_2$) was dissolved in mixed solvents of water (50 mL) under vigorous stirring for 5 min，then 5 mL alcohol solution of 0.1 g mL^{-1} P123 (alcohol was used to increase the solubility of P123) were added to, with vigorous stirring for another 5 min to ensure complete mixing. The solution were transferred into a Teflon-lined stainless autoclave. The autoclave was sealed and maintained at 150 °C for 24 h statically, and then was allowed to cool to room temperature naturally. Consequently, the white precipitated powder was obtained by filtration, washed by alcohol and distilled water several times. The sample was dried at 70 °C for 12 h, and then calcined at 600 °C in air for 4 h. Control experiments, as described above, but with the molar ratio of $CO(NH_2)_2/Al^{3+}$ (RUAl) being adjusted to 1.5:1 (Sam.1), 2.25:1 (Sam.2), 3:1 (Sam.3), 3.75:1 (Sam.4) at Vp123=5 and the amount of P123 (Vp123) being adjusted to 1 (Sam.5), 3 (Sam.6), 7 (Sam.7), 0 mL (Sam.8) at RUAl =1.5, were also undertaken to study the specific effect of the urea and P123 on the morphology.

Characterization

The crystal structure and phase purity of the product were examined by X-ray diffraction (XRD, D/max-2500, Cu-Kα radiation). An overview of the sample morphology was checked with a scanning electron microscope (SEM, JSM-7500F, JEOL) and transmission electron microscopy (TEM, JEM-2100, JEOL) analysis. Nitrogen adsorption and desorption isotherms were conducted at 77 K by using a Micrometrics ASAP-2420. Prior to the above measurements, the as-prepared samples had been degassed under vacuum at 300 °C for 400 min. Pyridine FTIR spectra were recorded on a Nicolet-6700 spectrometer. The samples were pressed into self-supporting discs, placed in an IR cell, and treated under vacuum (10^{-5} Torr) at 400 °C for 2 h. After cooling down to room temperature, the samples were exposed to pyridine vapor for 30 s. Then, IR spectra were recorded after evacuation (10^{-5} Torr) for 1 h at various temperatures.

Absorption treatment of Methyl orange

Treatment of adsorption performance was performed by adding 40 mg of as-prepared samples into 100 mL Methyl orange (40 mg L^{-1}) under vigorous stirring at room temperature. Analytical sample was taken from the suspension after desirable adsorption times and separated by filtration. The Methyl orange concentration was monitored by a UV-vis spectrophotometer (UV-2550, Shimadzu, Japan). The characteristic adsorptions around 466 nm were chosen to monitor the adsorption process and the C/C_0 was used to characterize the relative adsorption capacity (C_0 and C represent the initial concentration and concentration after equilibrium adsorption treatment, respectively).

Results and discussion

Structure property and morphology

Powder XRD was used to monitor the changes in the phase of the as-prepared and calcined samples. Fig.1 shows the wide-angle XRD patterns of the Sam.1 before (Fig.1a) and after calcination (Fig.1b). Fig.1a shows all detectable peaks in this pattern, which can be assigned to orthorhombic γ-AlOOH (JCPDS card no. 21-1307), the results demonstrate that all γ-AlOOH nanostructures are well-crystallized and no evidence could be found for the existence of other impurities in the products. The broaden diffraction peaks indicate that the as-obtained samples were composed of small crystals with a crystalline structure in nanometer scale. We obtained the γ-AlOOH with the urea, which used as a Brőnsted base for coprecipitation of metal ions and synthesis of metal-oxides or hydroxide with tuning the pH value of the medium remains relatively low throughout the reaction process. The procedures of AlOOH preparation can be described as follows[27,28]:

$NH_2CONH_2 + H_2O \rightarrow CO_2 + 2NH_3$ ---------- (1)

$NH_3 + H_2O \rightarrow NH_4^+ + OH^-$ ---------- (2)

$Al^{3+} + 3OH^- \rightarrow Al(OH)_3$ ---------- (3)

$Al(OH)_3 \rightarrow AlOOH + H_2O$---------- (4)

The virgin γ-Al_2O_3 (Fig.1b) (JCPDS card no. 10-0425) were fabricated by calcination of the as-prepared γ-AlOOH at 600 °C for 4 h, in agreement with a previous report[29] that the phase is yield via the dehydration process of AlOOH at temperatures between 400 °C and 700 °C.

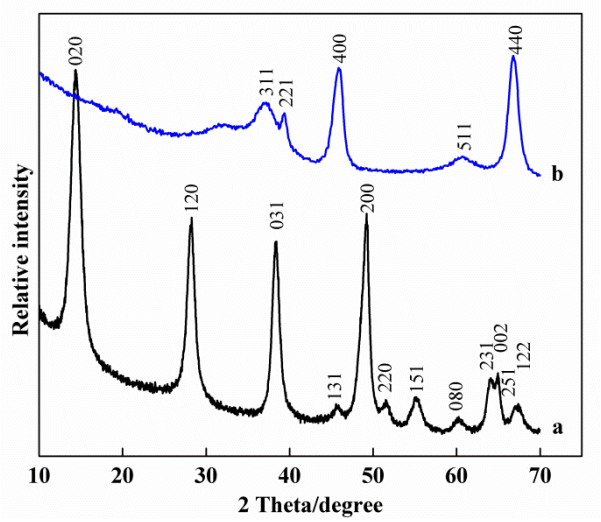

Fig.1. XRD patterns of Sam.1 before (a) and after calcination (b) under 600 °C for 4 h.

RSC Advances Accepted Manuscript

Fig.2 and Fig.S1 present SEM and TEM images of the 3D flower-like (Sam.1) γ-Al_2O_3 and γ-AlOOH nanostructures, respectively. Fig.2a-2b shows that well-defined 3D hierarchical flower-like γ-Al_2O_3 are self-assembled into the nanostructures with an mean size about 1.5~2 μm can be clearly observed. Moreover, no other morphologies can be observed, indicating a well-ordered 3D hierarchical flower-like morphology of the as-prepared γ-Al_2O_3. The TEM images of the γ-Al_2O_3 flower-like nanostructures are shown in Fig.2c-2d, which suggesting that the entire structure of the architectures were composed of several bunches of flake-like nanopetals with the lengths around 1 μm and 100 nm in width, respectively. These nanopetals with sharp edges and corners made of several aggregated nanoparticles which may be extremely useful for the high BET surface areas and high value of pore volume (see below). In addition, these nanopetals connected to each other via the centre to fabricate 3D flower-like hierarchical structures.

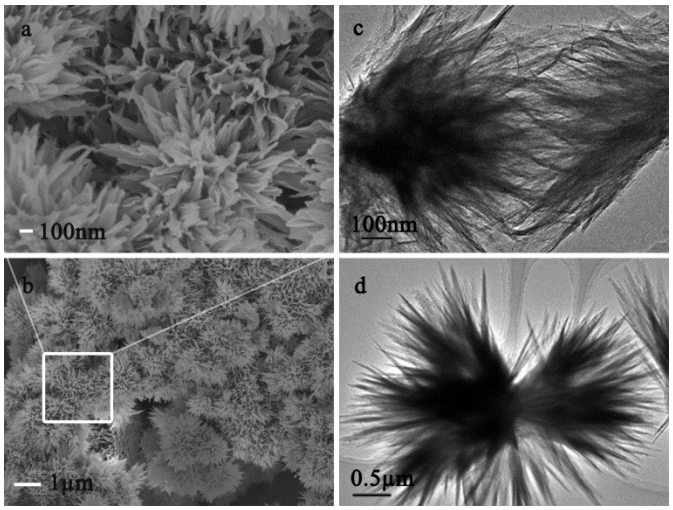

Fig.2. Typical SEM images (a-b) and TEM images (c-d) of the flower-like γ-Al_2O_3 (Sam.1): a, top-magnification image; b, low-magnification image;

It is significant to note that the 3D hierarchical flower-like nanostructures are considerable stable, even treated with the high temperature calcination, the integral morphology of the 3D hierarchical flower-like γ-AlOOH precursor nanostructures are not damaged after the calcination (as shown by Fig.2a and Fig.S1 (Supporting Information)). The size and morphology of γ-Al_2O_3 are extreme similar to those of the γ-AlOOH, indicating that the size and morphology can be well preserved during the phase-transformation from γ-AlOOH to γ-Al_2O_3.

Surface area and porosity

Fig.3 exhibits N_2 adsorption-desorption isotherms and corresponding pore-size distribution (inset) of flower-like (Sam.1) γ-Al_2O_3 (a) and γ-AlOOH (b), which exhibit similar Type IV shape isotherms with H1 hysteresis loops at relative pressures of P/P_0 above 0.35 and 0.45, respectively. The samples show almost the same adsorption and desorption branch as well as the pore-size distribution, indicating that they possess the similar structure, which is in consistent with the SEM and TEM images (Fig.2 and Fig.S1c). Accordingly, the corresponding pore-size distribution were relatively narrow, and the samples all shown a narrow pore-size distribution centring at about 4 nm. It is may be the result of the coexistence of the high uniform nanopetals and flower-like nanostructures (Fig.2), suggesting that the distribution of 4 nm originated from the nanopetals and flowers. The BET surface areas and the pore volumes of the flower-like γ-AlOOH and γ-Al_2O_3 are shown in Table S1. The BET surface areas were as high as 186 m^2/g, which is higher than that of the reported flower-like nanostructures[26]. After calcination, the BET surface areas drastically increased from 186 to 260 m^2/g due to the phase transformation within the aluminium species, meanwhile, the pore volume increased from 0.31 to 0.49 cm^3/g and the average pore width decreased from 8.6 to 7.3 nm.

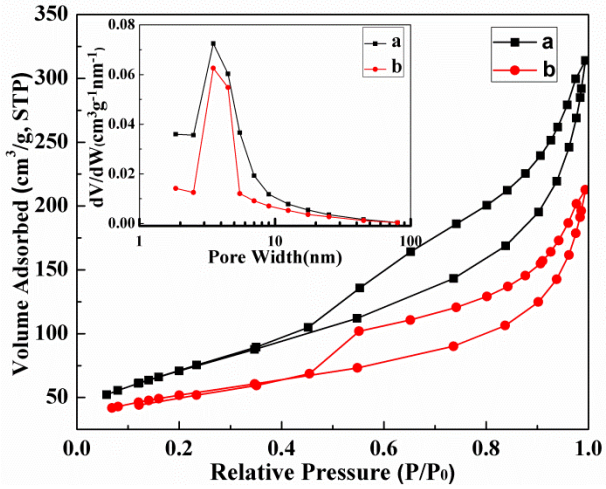

Fig.3. N_2 adsorption-desorption isotherms and corresponding BJH-pore size distribution (inset) of flower-like (Sam.1) γ-Al_2O_3 (a) and γ-AlOOH (b).

Surface acidity

It is well known that a alumina has considerable strong Lewis acidity (L acidity) and little Brőnsted acidity (B acidity) with the characteristic absorption peak at 1450 cm^{-1} and 1540 cm^{-1},

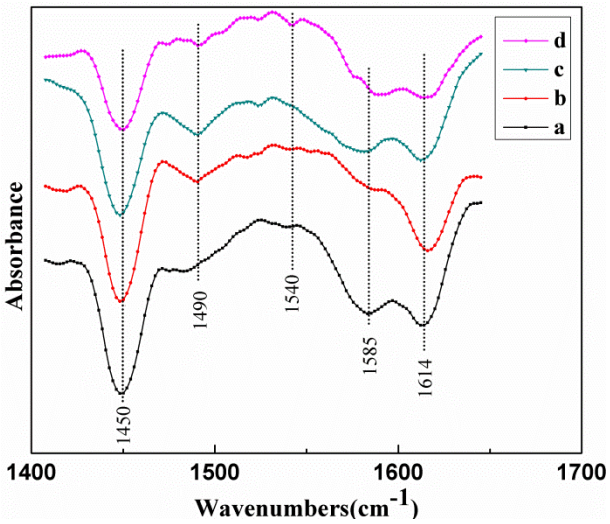

RSC Advances Accepted Manuscript

Fig.4. FTIR spectra of pyridine adsorption on the γ-Al_2O_3 samples after evacuation for 1 h at 160 °C. a, Sam.5; b, Sam.6; c, Sam.1; d, Sam.7.

respectively[30]. Fig.4 shows the FTIR spectra of samples after pyridine adsorption and evacuation at 160 °C, and the corresponding numbers of acid sites on the samples were shown in Table 1. The bands at 1450 and 1585 cm^{-1} are raised to the 8a and 19b modes of pyridine molecules interacting via hydrogen-bonding with the weakly acidic surface hydroxy-groups of γ-Al_2O_3 while the band at 1614 cm^{-1} are attributed to the same modes of pyridine molecularly coordinated with Al^{3+}, acting as Lewis acid sites. The band at 1490 and 1540 cm^{-1} are assigned to the 19a and 19b modes of pyridinium cations, associated to a total proton transfer from the Brőnsted acidic surface OH^- group to the basic molecule. The intensity of bands are in good agreement with the numbers of acid sites on the samples (Table 1). It is worth nothing that, the increasing amount of P123 have no regular relationship with the amount of total acid sites, while the Lewis acid sites reduced. Although the previous reports[31] claimed that the total acid sites decreased severely after the calcination treatments, in this work, the acid sites can be preserved by the addition of P123.

Table 1. The numbers of acid sites on the samples recorded at 160°C.

samples	Total acidity (mmol/g)	L acidity (mmol/g)	B acidity (mmol/g)
Sam.5	0.391	0.369	0.022
Sam.6	0.355	0.345	0.010
Sam.1	0.330	0.318	0.012
Sam.7	0.339	0.310	0.029

Effect on the morphology formation

The molar ratio of $CO(NH_2)_2/Al^{3+}$ (R_{UAl}) and amount of P123 (V_{p123}) were found to be critical in the morphology control (shown in Fig.5). First , Fig.2 and Fig.5a-5c show the

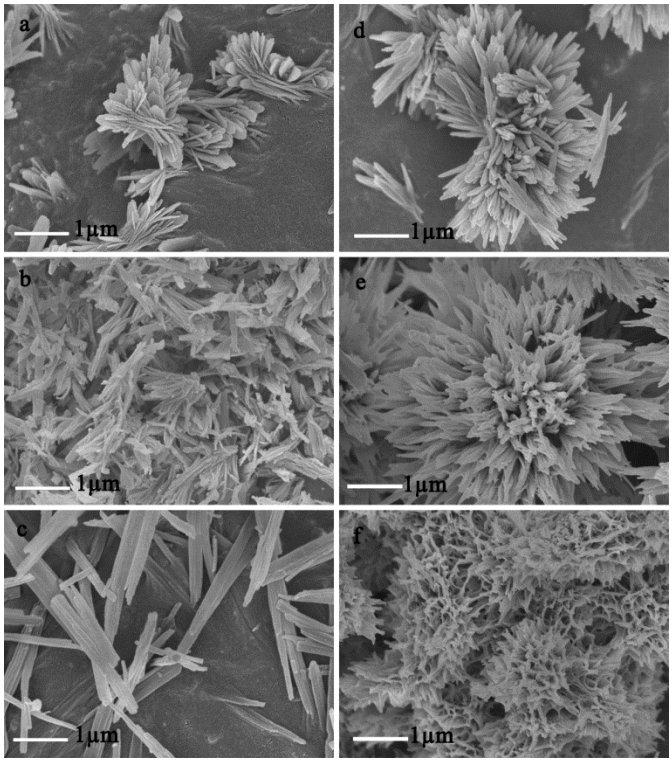

Fig.5 Typical SEM images of the γ-Al_2O_3 prepared under different synthesis conditions : (a) R_{UAl}=2.25, V_{p123}=5 (Sam.2); (b) R_{UAl}=3, V_{p123}=5 (Sam.3); (c) R_{UAl}=3.75, V_{p123}=5 (Sam.4); (d) V_{p123}=1, R_{UAl}=1.5 (Sam.5); (e) V_{p123}=3, R_{UAl}=1.5 (Sam.6); (f) V_{p123}=7, R_{UAl}=1.5 (Sam.7).

morphology of γ-Al_2O_3 obtained under the varied R_{UAl}, while other synthesis parameters keep a constant. As shown in the Fig.5a-b, a typical nanofilms obtained with R_{UAl}=2.25 (Sam.2) and R_{UAl}=3 (Sam.3), and Fig.5c presents a nanostrip with the widths ranging from 20 to 40 nm. With a increasing R_{UAl}, the morphology were changed from 3D hierarchical architectures (flower-like) to 1D architectures (nanostrip), which may raise by the PH value change of the solution. As show in the above equation (1)-(4), the pH values must gradually increase as the increasing of the OH^- content hydrolyzed by urea when the OH^- content were excess to react with the Al^{3+}. Generally, a slow hydrolysis of precursors may favour to the formation process of 1D oxide nanostructures such as nanowires and nanorods[32-33]. Thus, we can draw a conclusion that the increasing R_{UAl} hinder the hydrolysis of precursors, and result in the crystal growth in the form of nanofilms and nanostrips.

Second, Fig.2 and Fig.5c-5e show the morphology of the γ-Al_2O_3 obtained under the varied V_{p123}, while other synthesis parameters keep a constant. As shown in Fig.S2, there were only irregular particles obtained without the addition of P123. However, with the increasing P123 content, novel 3D flower-like nanostructures were gradually obtained (Fig.2 and Fig.5e-5f, Sam.1 and Sam.6-7) followed the faulty flower-like (Fig.5d). When the V_{p123}=1, a faulty (Fig.5d, Sam.5) flower-like nanostructures were obtained. Fig.5e shows the average diameter of flower-like nanostructures grew up to 2.5~3 μm as well as the lengths of the nanopetals grew up to 1~1.5 μm,

RSC Advances Accepted Manuscript

which have the similar nanopetals as the novel flower-like. On further increase the V_{p123} to 7.5, the increasing of the P123 amount increased the viscosity of the system, which would make the flowers swarm together by the connection of the nanopetals (Fig.2e). Generally, the addition of P123 could make the morphology grew to 3D hierarchical architectures.

It can be found that the increasing R_{UAl} could lead to the crystal growth in the formation of nanofilms or nanostrips, while the addition of P123 could have the morphology-alteration impact to 3D hierarchical architectures.

Formation mechanism

To further investigate the formation of flower-like nanostructure, the time-dependent experiments were also carried out by the SEM and TEM images (Fig.6 and Fig.S3). As shown in Fig.S3a, amorphous aluminum hydroxide nanorods with diameters around 30 nm appears. Prolonged to 10 h, the nanorods gradually self-assembled into lager flake-like nanopetals (Fig.6a) on the flowers (Fig.2). As the evolution proceeded, spindle-like were self-assembled (Fig.6b, 6d and inset) and, at the same time, some flowers were self-assembled by more nanopetals being self-assembled onto the spindles (Fig.6c and inset). In the higher magnification SEM image (Fig.6d), the self-assembled process can be clearly tell apart. Fig.3d and Fig.6b show the similar spindle-like nanostructures, indicating that when the reaction time prolonged to 12 h the dissolution procedure of P123 molecules in the system is the same as the system of Sam.5. In addition, the experiments suggested that the dissolution of P123 molecules were a rather slow process. After 16 h, The faulty flower-like nanostructures (Fig.6e-6f) were self-assembled via the aggregation of numerous nanopetals. A further increasing in the reaction time up to 18 h, led to the formation of more uniform flower-like (Fig.6g-6h and Fig.S3b).

The structural evolution was a long process , which might be the result of the hydrolysis of urea and the dissolution of P123 molecules. From the morphologies of the samples at different evolutionary stages, a possible three-plot formation mechanism is proposed. (I) First, the irregular AlOOH was formed from the previously formed $Al(OH)_3$ (equation 1-3) under the hydrothermal conditions. However, the amount of the AlOOH crystal at this time was small, and no precipitation was found, which is in well agreement with the time-dependent experiments of 6 h that we performed. As the OH^- content increased by the hydrolysis of urea, the irregular AlOOH particles tended to spilt for the distorted hydrogen bonds and interaction between the solvent molecules and the surface OH^- groups via hydrogen bonds, yields the 1D AlOOH nanorods (Fig.S3a) with the rolling mechanism[34-35]. (II) Then, the formed

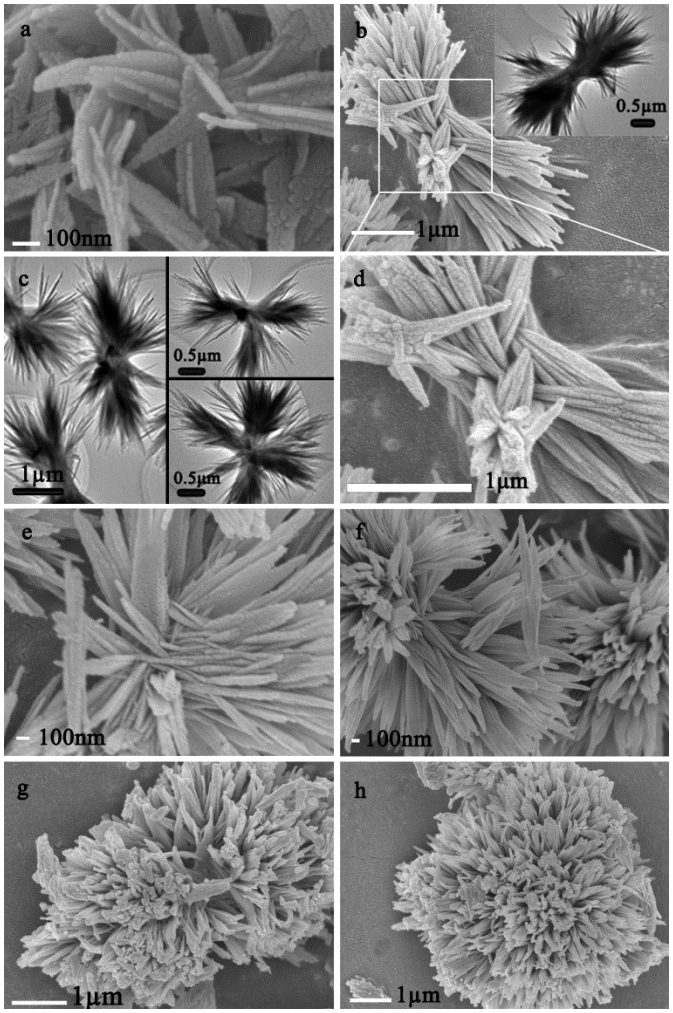

Fig.6. Morphology evolution of the samples prepared at different reaction stages at R_{UAl}=1.5, Vp123=5 and 150 ℃ for (a) 10 h, (b-d) 12 h,(e-f) 16h, (g) 18 h, and (h) 22 h. TEM images (c and the inset in b) were also displayed.

nanorods began to form nanopetals (Fig.6a), possibly via an oriented-attachment process[36]. (III) As the reaction proceeded, the P123 content was gradually increased in the reaction system and the number of P123 adsorbed on the surfaces of nanopetals was higher, which may result in self-assemble process of nanopetals into spindle-like structure (Fig.6b-6d and inset). It is believed that the flower-like ZnO[37] and CuS[38] structure are preferably formed from rods structure in order to minimize the interfacial free energy, which is also suitable for the formation of flower-like γ-Al_2O_3 structure. With a prolonged reaction time, the spindle-like finally self-assembled into novel flower-like (Fig.2 and Fig.6g-6h) by Vander Waals forces and the hydrogen bonding[36], which have the lower interfacial free energy. Our control experiments and time-dependent experiments agree well with the self-assembly formation mechanism of the flower-like nanostructure, suggesting the three-plot formation mechanism can be described as following Fig.7.

RSC Advances Accepted Manuscript

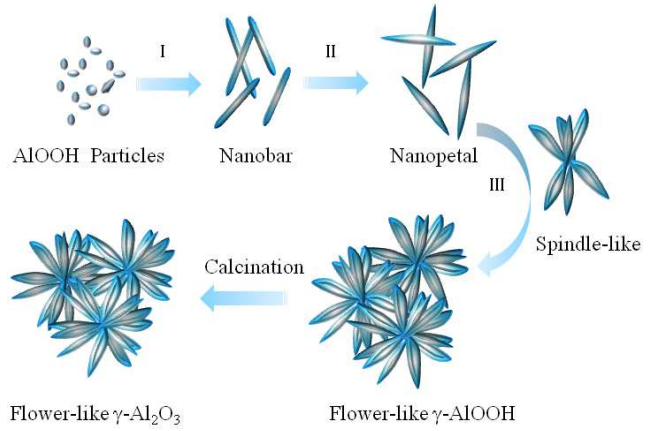

Fig.7. Schematic illustration of the formation of the flower-like γ-Al_2O_3.

Absorption application in water for Methyl orange

The as-prepared flower-like γ-Al_2O_3 samples were used as adsorbents for potential application in water treatment. Owing to their unique hierarchical porous structure and textual properties[39-42]. As show in Fig.8B, it is clear that over 90.0% of the Methyl orange had been adsorbed at room temperature after only 2-4 min, and an equilibrium established within 4 min. With the increasing of V_{p123}, the adsorption behaviors change slightly (Fig.8B.b-d) except for the Sam.5. As show in Fig.5d-5f and Fig.2, the faulty and uniform flower-like nanostructures may be a key effect on the adsorption behaviors, which exhibit the similar pore structure property (Table S1). In contrast, the commercial γ-Al_2O_3 shown much lower adsorption efficiency (Fig.8B.e) than the flower-like nanostructures due to the novel morphology. However, the flower-like γ-AlOOH (Fig.8B.b*) exhibited an lowest adsorption efficiency, which had unique hierarchical structure, indicating that the γ-AlOOH have weaker adsorption properties than γ-Al_2O_3[41-42]. The enhanced adsorption properties of γ-Al_2O_3 are mainly affected by the coordination of the unique hierarchical structure and chemical composition.

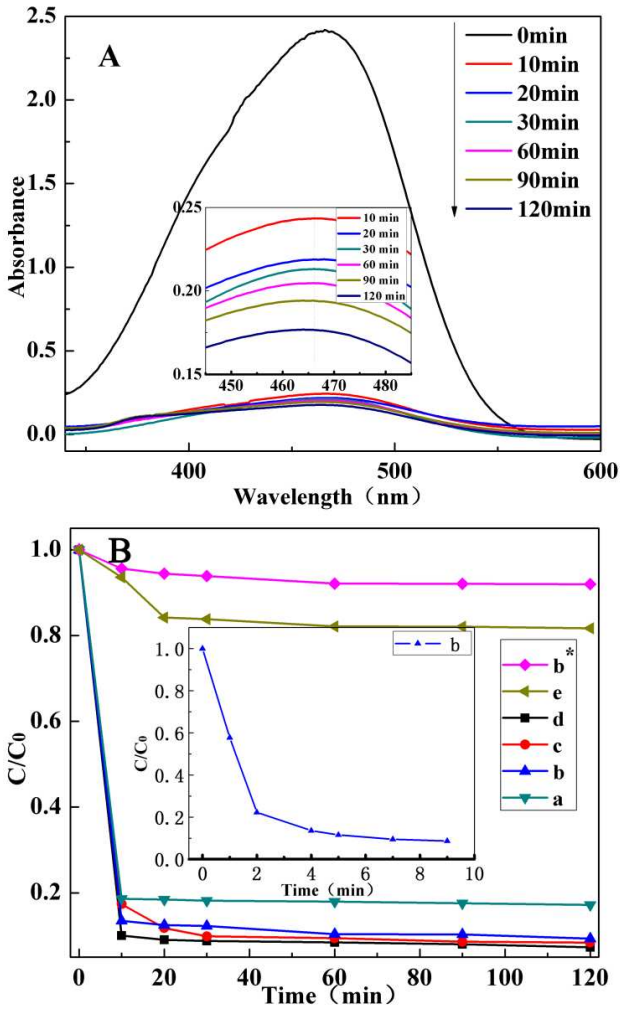

Fig.8. UV-vis absorption spectra of Methyl orange in the presence of the γ-Al_2O_3 (Sam.1) after time intervals (A) and the adsorption rates (B) on different samples: a, Sam.5; b, Sam.1; c, Sam.6; d, Sam.7; e, commercial γ-Al_2O_3; b*, γ-AlOOH obtained before the calcination of the corresponding Sam.1 (b). The inset in Fig.8A and 8B show the partial enlarged spectra and an accurate measurement with a short time scale, respectively.

Conclusion

A series of nanofilm, nanostrip, spindle-like and flower-like γ-AlOOH and γ-Al_2O_3 nanoarchitectures were successfully synthesized by a facile method. The influence in morphology control were studied by altering the amount of P123 (V_{p123}) and molar ratio of $CO(NH_2)_2/Al^{3+}$ (R_{UAl}), implying that the increasing R_{UAl} could lead to the crystal growth in the formation of nanofilms or nanostrips and the addition of P123 could have the morphology-alteration impact to 3D hierarchical architectures. Moreover, the possible self-assembled formation mechanism were put forward by combining the control experiments and time-dependent experiments. The morphology of the flower-like nanoarchitectures was strongly dependent on the experimental conditions including the molar ratio of $CO(NH_2)_2/Al^{3+}$, the amount of P123 and the reaction time. Further adsorption investigation indicates that the flower-like γ-Al_2O_3 have good adsorption properties involving with Methyl orange. The novel flower-like γ-AlOOH and γ-Al_2O_3 are promising candidates for industrial application, such as adsorbents, catalyst, catalyst supports, ceramic, and optical nanodevices.

Acknowledgement

This work was financially supported by the SINOPEC (No. 113027). The authors are grateful to Dr. L. Wang for helpful discussions.

RSC Advances Accepted Manuscript

Notes and reference

[a] School of Chemistry and Material Science, Liaoning Shihua University, Fushun, 113001, China.
[b] Fushun Research Institute of Petroleum and Petrochemicals, SINOPEC, Fushun, 113001, China.
*Corresponding author. Tel: +86 24 56389578; Fax: +86 24 56429551
E-mail address: fengxiangling.fripp@gmail.com

1 S. F. Xie, B. J. Zheng, Q. Kuang, X. Wang, Z. X. Xie and L. S. Zheng, CrystEngComm., 2012, 14, 7715.
2 (a) J. S. Hu, L. S. Zhong, W. G. Song and L. J. Wan, Adv. Mater., 2008, 20, 2977; (b) D. F. Zhang, H. Zhang, L. Guo, K. Zheng, X. D. Han and Z. Zhang, J. Mater. Chem., 2009, 19, 5220.
3 P. Yu, X. Zhang, D. L. Wang, L. Wang and Y. W. Ma, Cryst. Growth Des., 2009, 9, 528.
4 Y. Q. Wang, G. Z. Wang, H. Q. Wang, W. P. Cai, C. H. Liang and L. Zhang, Nanotechnology., 2009, 20, 155604.
5 A. M. A. Cruz and J. G. Eon, Appl. Catal. A-Gen., 1990, 167, 203.
6 Mishra. D, Anand. S, Panda. R. K and Das. R. P, Mater. Lett., 2000, 42, 38.
7 Y. Kim, C. Kim, I. Choi, S. Rengaraj and J. Yi, Environ. Sci. Technol., 2004, 38, 924.
8 K.V. P. M. Shafi, A. Ulman, J. Lai, N. L. Yang and M. H. Cui, J. Am. Chem. Soc., 2003, 125, 4010.
9 B. E . Yoldas, J. Mater. Sci., 1975, 10, 1856.
10 Music. S, Dragcevic. O and Popovic. S, Mater. Lett., 1999, 40, 269.
11 Raybaud. P, Digne. M, Iftimie. R, Wellens. W, Euzen. P and Toulhoat. H, J. Catal., 2001, 201, 236.
12 P. Kim, J. B. Joo, H. Kim, W. Kim, Y. Kim, I. K. Song and J. Yi, Catal. Lett., 2005, 104 , 181.
13. S. M. Kim, Y. J. Lee, J. W. Bae, H. S. Potdar and K. W. Jun, Appl. Catal. A-Gen., 2008, 348, 113.
14 Dupont. J, de Souza. R. F and Suarez. P. A. Z, Chem. Rev., 2002, 102, 3667.
15 Z. R. Zhang, R.W. Hicks, T. R. Pauly and T. J. Pinnavaia, J. Am. Chem. Soc., 2002, 124, 1592.
16 G. Paglia, E. S. Bozin, S. J. L. Billinge, Chem. Mater. 2006, 18, 3242.
17 D. Kuang, Y. P. Fang, H. Q. Liu, C. Frommen and D. Fenske, J. Mater. Chem., 2003, 13, 660.
18 (a) D. Deng, R. Tang, X. Liao and B. Shi, Langmuir., 2008, 24,368. (b) W. Q. Cai, H. Q. Li and Y. Zhang, Colloids Surf. A., 2007, 295,185. (c) B. Gong, Q. Peng, J. S. Jur, C. K. Devine, K. Lee and G. N. Parsons, Chem. Mater., 2011, 23, 3476.
19 T. B. He, L. Xiang and S. L. Zhu, Langmuir., 2008, 24, 8284.
20 Z. Y, Tang, Kotov. N. A and Giersig. M, Science, 2002, 297, 237.
21 X. Y. Chen, H. S. Huh and S. W. Lee, Nanotechnology., 2007, 18, 285608.
22 L. Zhang and Y. J. Zhu, J. Phys. Chem. C., 2008, 112, 16764.
23 X. Wang, P. Hu, F. L. Yuan and L. J. Yu, J. Phys. Chem. C., 2007, 111, 6706.
24 S. Y. Gao, H. J. Zhang, X. M. Wang, R. P. Deng, D. H. Sun. and G. L. Zheng, J. Phys. Chem. B., 2006, 110, 15847.
25 W. Q. Cai, J. G. Yu and S. Mann, Microporous Mesoporous Mater., 2009, 122, 42.
26 J. Zhang, S. J. Liu, J. Lin, H. S. Song, J. J. Luo, E. M. Elssfah, E. Ammar, Y. Huang, X. X. Ding, J. M. Gao, S. R. Qi and C. C. Tang, J. Phys. Chem. B., 2006, 110, 14249.
27 W. H. R. Shaw and J. J. Bordeaux, J. Am. Chem. Soc., 1955, 77 , 4729.
28 S. Ramanathan, S. K. Roy, R. Bhat, D. D. Upadhyaya and A. R. Biswas, Ceram. Int., 1997, 23 , 45.
29 Chanakya. Misra, American Chemical Society (Washington DC)., 1986.
30 (a) Parry. E. P, Journal of Catalysis., 1963,2, 371. (b) Busca G, Catal. Today., 1998, 41, 191.
31 X. R. Huang and X. H. Li, Journal of Molecular Catalysis., 2001, 15, 6.
32 Y. Wan and D. Y. Zhao, Chem. Rev., 2007, 107, 2821.
33 Q. S. Huo, D. Y. Zhao, J. L. Feng, Weston. K, Buratto. S. K, Stucky. G. D, Schacht. S and Schuth. F, Adv. Mater., 1997, 9, 974.
34 Pierre A. C and Uhlmann D. R. J, Non-Cryst. Solids., 1986, 82, 271.
35 Jillian F. Banfield, Susan A. Welch, H. Z. Zhang, and Tamara Thomsen Ebert, Science., 2000, 289, 751.
36 Penn R. L and Banfield J. F, Science., 1998, 281, 969.
37 R. X. Shi, P. Yang, J. R. Wang, A. Y. Zhang, Y. N. Zhu, Y. Q. Cao and Q. Ma, CrystEngComm., 2012, 14, 5996.
38 H. Qi, J. F. Huang, L. Y. Cao, J, P, Wu, Key Engineering Materials., 2012, 512, 265.
39 J. B. Lian, X. C. Duan, J. M. Ma, P. Peng, T. I. Kim and W. J. Zheng, ACS Nano., 2009, 3, 3749.
40 J. B. Fei, Y. Cui, X. H. Yan, W. Qi, Y. Yang, K. W. Wang, Q. He and J. B. Li, Adv. Mater., 2008, 20, 452.
41 Y. Wang, W. Li, X. L. Jiao and D. R. Chen, J. Mater. Chem. A., 2013, 1, 10720.
42 W. Q. Cai, Y. Z. Hu, J. Chen, G. X. Zhang and T. Xia, CrystEngComm., 2012, 14, 972.

RSC Advances Accepted Manuscript